In situ evidence that mast cells release mutant NLRP1 in keratoacanthomas from multiple self-healing palmoplantar carcinoma

Alexandra Dobre[1,2], Tudor E. Fertig[1,3]*, Andrei M. Niculae[1,3,4], Adelina M. Cohn[1,5], Antoanela Curici[1,6], Razvan T. Andrei[6,7], Daciana S. Marta[3,8], Victor E. Peteu[3], Roua G. Popescu[9,10], George C. Marinescu[9,10], Gabriela Turcu[1,7,11], Ana M. Forsea[1,2,12], Daniela A. Ion[1], Mihaela Gherghiceanu[1,3]**, Roxana I. Nedelcu[1,11]**

[1] Carol Davila University of Medicine and Pharmacy, Bucharest, Romania

[2] Elias University Emergency Hospital, Dermatology, Bucharest, Romania

[3] Victor Babeş National Institute of Pathology, Bucharest, Romania

[4] Pathology Department, "Dr. Carol Davila" Central Military Emergency University Hospital, Bucharest, Romania

[5] Laboratoire National De Santé, Dudelange, Luxembourg

[6] Synevo Romania, Bucharest, Romania

[7] Colentina Clinical Hospital, Bucharest, Romania

[8] Faculty of Medicine, Titu Maiorescu University, Bucharest, Romania

[9] Asociația Independent Research, Bucharest, Romania

[10] Blue Screen SRL, Bucharest, Romania

[11] Derma 360 Clinic, Bucharest, Romania

[12] Health and Medical University Potsdam, Germany

*Corresponding author: Tudor Emanuel Fertig, +4021 319 2732, Dionisie Lupu 37, Bucharest 030167, emanuel.fertig@umfcd.ro

ABSTRACT

Multiple self-healing palmoplantar carcinoma (MSPC) is a rare syndrome characterized by germline mutations of the inflammasome sensor protein NLRP1, causing its constitutive activation and ultimately, IL1β-driven inflammation. Because NLRP1 is well expressed in human skin, the effect is aberrant keratinocyte proliferation with the appearance of characteristic, recurrent keratoacanthomas (KAs) on palms and soles. We aimed to clarify the subcellular localization of mutant NLRP1 in the skin of a MSPC patient with plantar KAs and a sudden psoriasis-like eruption. Skin biopsies from the MSPC patient and healthy controls were processed for immunohistochemistry and immunoelectron microscopy. We found for the first time that NLRP1 localized to mast cell (MC) granules in both healthy and lesional skin. Moreover, MCs expressing the A66V pathogenic variant of NLRP1 overpopulated plantar KAs of a MSPC patient, infiltrated the epidermis and degranulated, a behavior not seen in the psoriasis-like lesion (PLL) from the same patient, nor in healthy skin. The released granules had higher NLRP1 content than MSPC-PLL and also contained NLRP3 and IL1β. Overall, this data suggests that MCs can contribute to the pathogenesis of KAs in MSPC, which opens a new area of research in NLRP1-related syndromes.

40 **INTRODUCTION**

41 NLRP1 (NLR family pyrin domain containing 1) is a cytosolic sensor protein with a major role
42 in innate immunity. In response to pathogens or other stress signals, NLRP1 can participate in
43 the formation of an intracellular protein complex termed "inflammasome"[1], which allows
44 activation of caspase-1, followed by IL1β secretion and pyroptotic cell death[2].

45 In humans, NLRP1 pathogenic variants can lead to a variety of clinical syndromes depending
46 on the affected protein domain, mainly involving skin, cornea and lungs[3–6]. Multiple self-
47 healing palmoplantar carcinoma (MSPC) is an extremely rare such syndrome, characterized by
48 recurrent keratoacanthomas (KAs) that develop on palmoplantar skin and sporadically on other
49 epithelia lacking hair follicles[7]. Responsible are either one of three germline heterozygous
50 mutations (A54T, A66V, M77V) affecting the pyrin domain (PYD) of NLRP1, causing
51 spontaneous self-oligomerization of the protein, aberrant inflammasome activation and
52 subsequent proliferation of affected keratinocytes[7].

53 Keratinocytes are known as the main NLRP1 reservoir in human skin[7–10], however
54 granulocytes, lymphocytes, macrophages and dendritic cells also express NLRP1[11]. RNA-seq
55 data from the Human Protein Atlas indicates basophils as having the highest potential for
56 NLRP1 expression among immune cells[12,13].

57 Mast cells (MCs) are tissue-resident immune cells of hematopoietic origin, which differentiate
58 from a basophil-MC common progenitor. Although not yet described to contain NLRP1, MCs
59 contain NLRP3 within secretory granules and are capable of producing IL1β following NLRP3
60 inflammasome activation[14,15]. Mutations of NLRP3 cause it to become constitutively activated
61 in MCs, initiating overproduction of IL1β. In humans, this contributes to a spectrum of clinical
62 entities named cryopyrin-associated periodic syndromes (CAPS), in which the skin, joints and
63 central nervous system can be affected[14,16].

64 We report for the first time that skin MCs harbor NLRP1 within granules. We further show
65 massive and specific degranulation of MCs in different KAs of a MSPC patient with
66 $NLRP1^{A66V}$ and suggest that release of granules containing this hyperactive NLRP1 variant
67 contributes to the pathogenesis of KAs in this syndrome.

68 **MATERIALS & METHODS**

69 **Patients and samples**

70 All subjects gave written informed consent prior to biopsy. Four samples were collected from
71 a single MSPC patient with NLRP1^{A66V}: three different KAs from plantar regions (in 2016,
72 2023 and 2025) and a sample from a psoriasis-like plaque on the abdomen (in 2023). Biopsies
73 were collected from the elbow region of two clinically healthy volunteers. The study included
74 6 archived formalin-fixed paraffin-embedded (FFPE) KA specimens, from different patients
75 with no clinical history of MSPC. A human lymph node FFPE specimen was included as
76 NLRP1 positive control. This study was performed in conformity with the Declaration of
77 Helsinki and received approval from the ethics committees at Victor Babeș National Institute
78 of Pathology and Elias University Emergency Hospital, Bucharest, Romania.

79 **Light microscopy and immunohistochemistry**

80 Hematoxylin-eosin was done by routine protocol. IHC with the primary antibody of interest
81 (**Table S1**) was done using an Autostainer Link 48, following manufacturer specifications
82 (Dako, Agilent Technology, US). An isotype control and omission of primary antibody were
83 used to verify non-specific binding. Digital slides were obtained using an automated slide
84 scanner (Aperio AT2, Leica Biosystems, US).

85 **Immunoelectron microscopy**

86 Biopsies were fixed in a solution comprising 4% paraformaldehyde, 0.5% glutaraldehyde, and
87 1.4% sucrose (pH 7.4), then embedded in London Resin White (LR White, Agar Scientific,
88 UK). Ultra-thin sections were mounted on formvar and carbon-coated nickel grids, then
89 incubated with the primary antibody of interest (**Table S1**) and a gold-conjugated secondary
90 antibody at 1:50 dilution (Aurion, The Netherlands). Negative controls had primary antibodies

omitted and an isotype control was used to exclude nonspecific binding to MC Fc receptors. A blocking solution for goat antibodies was used to reduce nonspecific binding (Aurion, The Netherlands). Imaging was done using a 4×4k Ceta camera, on a Talos 200C transmission electron microscope (Thermo Fisher Scientific, US).

Immunoelectron tomography

This method allowed simultaneous labeling with up to three different primary antibodies. Briefly, LR White sections (300 nm) were adhered to nickel grids precoated with 0.01% poly-L-lysine and without formvar or carbon. For double-labeling, grids were incubated on each side, consecutively, with two primary antibodies raised in different species (mouse and rabbit, **Table S1**). For triple-labeling, grids were incubated on one side with a mixture of two antibodies raised in different species (mouse and rabbit, **Table S1**), then either a rabbit or mouse primary antibody was used on the other side. To facilitate identification, secondary antibodies had different colloidal gold diameters for each target (6, 10 and 15 nm, Aurion, The Netherlands). Absence of cross-contamination between section faces was verified by immunolabeling control grids on one side, while the other side was incubated with PBS. Acquisition of single axis tilt series, tomographical reconstruction and segmentation were done using IMOD-eTomo[17], as described elsewhere[18].

Data analysis

Quantification of MCs was performed on tissue sections stained for tryptase. For each case, tryptase-positive cells were manually counted in ten consecutive high-power fields (HPF, 40× objective), starting from a hotspot. Each experimental group included approximately 27 observations ($n \approx 27$ per group). To quantify the NLRP1 content of MC granules, cells were first identified on randomly selected ultrathin sections from the MSPC and healthy skin specimens, immunolabeled under identical conditions. Entire MCs were imaged, then colloidal

gold was counted on all granules of each cell. Each experimental group included approximately 1,058 observations ($n \approx 1{,}058$ per group).

Statistical analyses were performed using one-way ANOVA, followed by Tukey's post hoc test for pairwise comparisons between groups. Statistical significance is presented only for comparisons with p-values $< .05$. The post hoc statistical power for the applied tests was 1. All analyses and graphical representations were generated using R software (version 4.4.1).

121 **RESULTS**

122 **MSPC patient develops overlapping psoriasis-like skin condition**

123 A 49-year-old male with a history of multiple central hyperkeratotic lesions on the palms and
124 soles (**Figure 1a**) in the context of a previously diagnosed MSPC with the A66V pathogenic
125 variant of NLRP1[7], presented with symmetrically distributed and well-defined erythematous-
126 squamous plaques, some with erosions and crusting. These initially appeared on the dorsal feet
127 and later spread to the extremities, trunk and head (**Figure 1b**). An infection was ruled out
128 because of unresponsiveness to antibiotics/antifungals. Instead, an overlap of allergic contact
129 dermatitis with psoriasis was suspected due to: (a) histopathological diagnosis of psoriasis on
130 an abdominal plaque (**Figure 1c**), (b) atypical development and clinical presentation of
131 plaques, (c) positive patch-tests to lanolin alcohol and nickel(II) sulfate hexahydrate, (d) good
132 response of lesions to oral corticotherapy and lanolin-free moisturizers, (e) IgE approximately
133 twice the normal value at presentation, which normalized after treatment, and (f) no recurrence
134 after corticotherapy.

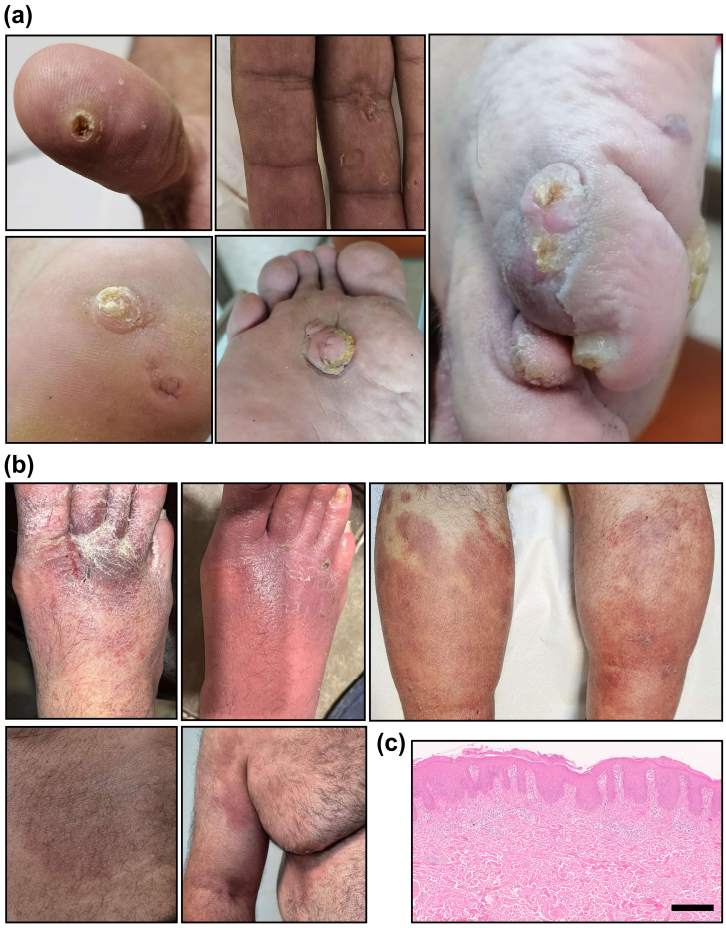

Figure 1. Clinical features of a patient with multiple self-healing palmoplantar carcinoma (MSPC). (a) Keratoacanthomas at different stages of evolution on the palmar and plantar surfaces. **(b)** Sudden development of poorly-defined erythemato-edematous plaques with erosions and scales on the dorsal feet. This evolved to a widespread eruption of well-defined erythemato-squamous plaques, including on the lower limbs and trunk. Some plaques resembled psoriasis. **(c)** Light microscopy (HE) of abdominal lesion from MSPC patient, showing relatively thin suprapapillary epidermis, psoriasiform epidermal hyperplasia with focal parakeratosis and hypogranulosis. There are neutrophil collections in the mounds of parakeratosis and moderate perivascular lymphocytic infiltrate in the superficial dermis. Images are published with patient consent. Scale bar = 300 µm.

146 **Degranulating MCs accumulate in MSPC-KAs**

147 Given that the psoriasis-like lesions (PLL) appeared in a patient with MSPC, we aimed to
148 understand how the lesional microenvironment and subcellular distribution of NLRP1^{A66V}
149 differed when compared to three plantar KAs from the same patient (biopsied 7 years prior,
150 concomitantly and 2 years after MSPC-PLL diagnosis) and to wild-type NLRP1 in the skin
151 from a healthy control.

152 First, we confirmed the presence of NLRP1 by mass spectrometry, in all samples, as identified
153 by at least two tryptic peptides having at least 2 transitions (MS2, resulted by collision induced
154 dissociation) (**Figure S1, Table S2**).

155 Then, we used immunohistochemistry (IHC) to look at the tissue distribution of NLRP1^{A66V} in
156 the three MSPC-KAs. As reported[7], keratinocytes were positive for NLRP1, with a nucleo-
157 cytoplasmic staining pattern and the intensity gradually decreasing towards the upper
158 epidermal layers (**Figure 2a**). Unexpectedly however, NLRP1 staining was more intense in the
159 dermis than the epidermis, with specific cell populations presenting a granular distribution
160 within the cytoplasm (**Figure 2a, top row inset**). Inversely, NLRP1^{A66V} expression was highest
161 in the epidermis of the MSPC-PLL sample, but comparatively reduced in the dermis, mainly
162 clustering around blood vessels (**Figure 2a**). Healthy skin showed the least NLRP1 staining
163 intensity in both epidermis and dermis (**Figure 2a**), although the granular distribution persisted
164 in cells surrounding blood vessels. Staining of immune cell granules by NLRP1 was confirmed
165 on a human lymph node specimen (**Figure S2a**), whereas the isotype control did not bind.

166 To investigate whether some of the numerous NLRP1-positive cells in the MSPC-KA dermis
167 were MCs, we stained using tryptase and CD117/c-kit (**Figure 2a**). Indeed, KA samples from
168 the MSPC patient had significant MC accumulation (27.2/mm^2), above MSPC-PLL
169 (17.5/mm^2) or healthy skin (7.6/mm^2) (**Figure 2b**). In MSPC-KAs but not MSPC-PLL, MCs
170 frequently infiltrated epidermal layers (**Figure 2a, middle row inset**).

171 Under higher magnification we observed that MCs in MSPC-KAs, but not MSPC-PLL, were
172 degranulated. Tryptase-positive granular material was widely distributed within connective
173 tissue, but also taken up in the epidermis, up to and including the spinous layer (**Figure 2c**).
174 To verify if this is a characteristic of all KAs or if this was restricted to the three MSPC-KAs
175 in this study, we used tryptase staining on six KAs from patients not diagnosed with MSPC
176 (**Figure S2b**). As expected[19], these presented MCs in higher numbers (13/mm^2) than healthy
177 skin, however below counts in MSPC-KAs and even MSPC-PLL (**Figure 2b**). Importantly, we
178 could not identify MC epidermal infiltration, nor significant MC degranulation, indicating their
179 distinct contribution in MSPC-KA pathogenesis.
180 The MSPC patient was negative for the D816V KIT pathogenic variant in whole blood and had
181 normal serum tryptase (<11.4 µg/L), limiting the possibility of MC neoplastic transformation.

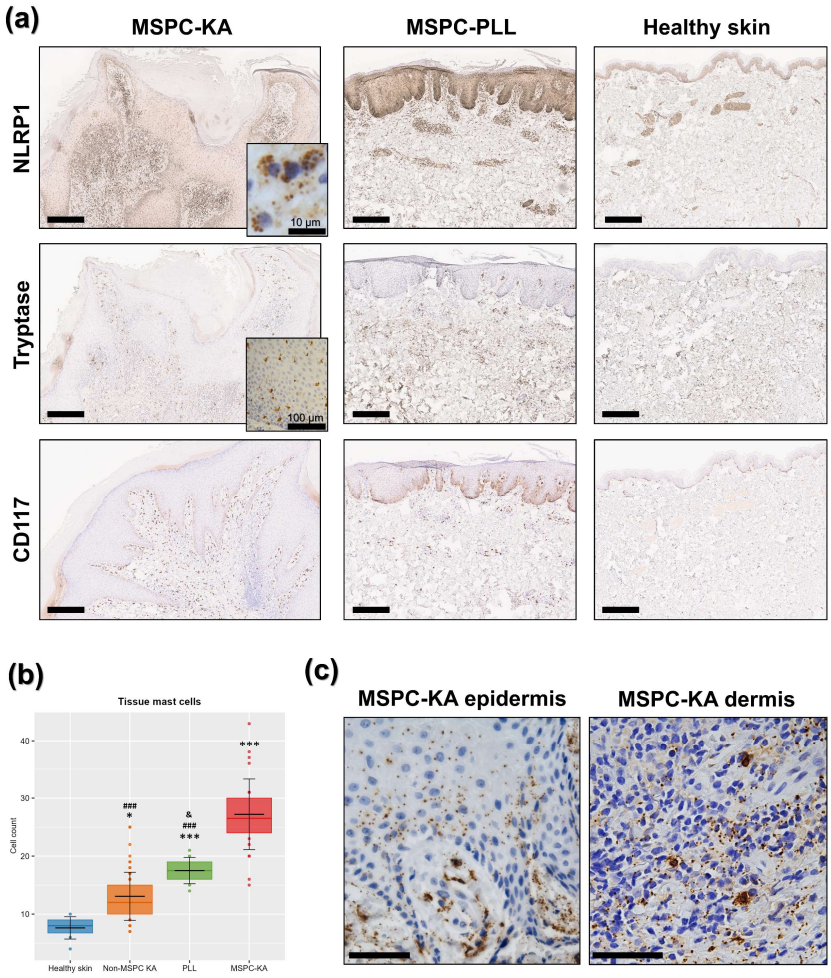

182

183 **Figure 2. Immunohistochemistry of keratoacanthomas (KAs) in multiple self-healing**
184 **palmoplantar carcinoma (MSPC). (a)** In MSPC-KAs, NLRP1^{A66V} was more highly
185 expressed in the dermis and was concentrated in cell granules **(top row inset**, scale bar = 10
186 µm**)**. In the psoriasis-like lesion (MSPC-PLL), NLRP1^{A66V} was overrepresented in the
187 epidermis. CD117 and tryptase staining demonstrated more mast cells (MCs) in MSPC-KAs,
188 including epidermal infiltration **(middle row inset,** scale bar = 100 µm**)**. Scale bars = 300 µm.
189 **(b)** Quantification of MCs in the analysed samples, presented as means ± standard deviation
190 (SD). Statistical significance is shown against healthy skin—*, MSPC-KA group—#, and the
191 non-MSPC KA group—&, where */& $p < .05$; ***/### $p < .001$. **(c)** MCs in MSPC-KAs were
192 degranulated, with granular material dispersed in epidermis and dermis. Scale bars = 50 µm.

193 **NLRP1 localizes to MC granules**

194 For more precise subcellular localization of NLRP1 we employed IEM. Morphologically, most
195 MCs from MSPC-KA were degranulated, ranging from having empty granules and granules
196 fused with the plasma membrane, to complete fragmentation of cells, with release of clumps
197 of granular complexes in the extracellular space (**Figure 3a**). By contrast, MCs from MSPC-
198 PLL and healthy skin had typical appearance (intact granule architecture, presence of plasma
199 membrane folds) and localized in proximity of blood vessels (**Figure 3b,c**).

200 Using two different, commercially available anti-NLRP1 antibodies, we demonstrated that
201 NLRP1 accumulates in granules of MCs from both lesional and healthy skin, regardless of
202 granule morphology and degranulation status of the cell, indicating NLRP1 is a ubiquitous
203 component of skin MCs (**Figure 3a,c and inset**). By contrast, an isotype control did not bind
204 (**Supplementary Figure 3a**). Next, we asked whether there are differences in MC NLRP1
205 content between samples, so we manually counted and averaged colloidal gold per granule,
206 under identical immunolabeling conditions. In this context, this method of quantification was
207 more precise than mass spectrometry of tissue lysates, as it measured protein content in the
208 subcellular compartment of interest, unbiased by overall density of MCs in tissue. We found
209 that NLRP1^{A66V} from MSPC-KA was overrepresented compared to NLRP1^{A66V} in MSPC-PLL
210 or wild-type NLRP1 in healthy skin (**Figure 3d**), further suggesting MCs may serve as a
211 reservoir of hyper-reactive NLRP1^{A66V} during MSPC-KA pathogenesis. Interestingly, MC
212 granules in MSPC-PLL had lower NLRP1 content than healthy skin, although the significance
213 of this is unclear.

214 In accordance with IHC, NLRP1 was also localized in keratinocytes in all samples, however it
215 unexpectedly clustered around intermediate filaments and desmosomes (**Figure S3b**).

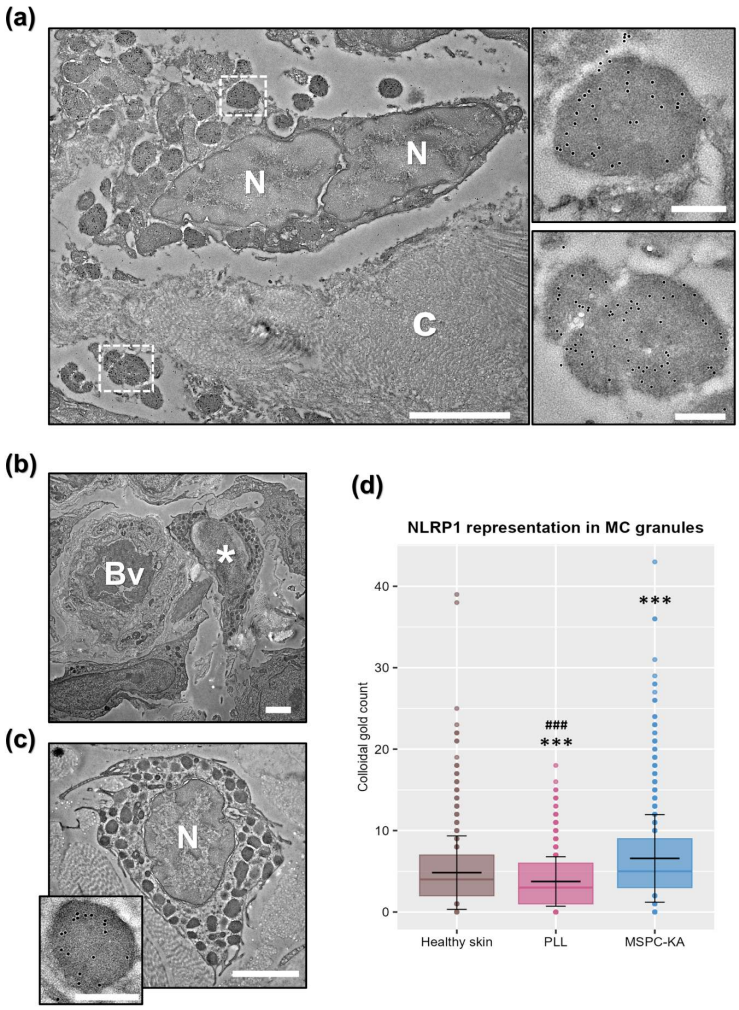

Figure 3. NLRP1 is ubiquitous in skin mast cell (MC) granules. (a) MCs in keratoacanthomas (KAs) from a multiple self-healing palmoplantar carcinoma (MSPC) patient were degranulated. Scale bar = 2 µm. *c - collagen, N - nucleus.* MC granules in MSPC-KA presented NLRP1^{A66V} accumulation, as exemplified by higher magnifications of boxed areas. Gold labeling is seen as black dots. Scale bars = 250 nm. **(b)** MCs from a psoriasis-like lesion (MSPC-PLL) were morphologically normal (*) and clustered around blood vessels (Bv). Scale bar = 2 µm. **(c)** Normal MC in healthy skin presenting NLRP1 in granules **(inset**, scale bar = 250 nm**)**. Scale bar = 2 µm. **(d)** Quantification of colloidal gold demonstrated MCs in MSPC-KA had more NLRP1 (means ± standard deviation). Statistical significance is shown against healthy skin—*, and MSPC-KA—#, where ***/### $p < .001$.

227 **NLRP1 and NLRP3 can colocalize in MC granules**

228 MCs are known to contain all components of the NLRP3 inflammasome and to secrete IL1β in
229 a NLRP3-dependent manner[14,15]. Given our finding that NLRP1^{A66V} is present in MC granules
230 from the MSPC patient, we were curious whether it spatially overlaps with NLRP3 and if it
231 could therefore share elements of the inflammasome machinery during activation. First, we
232 labeled MSPC-KA against pro-IL1β/IL1β (hereafter IL1β) and found it well represented in
233 both intracellular MC granules and in MC-derived extracellular granular material **(Figure 4a**
234 **and inset)**. This demonstrated that MCs in MSPC-KA secrete this pro-inflammatory cytokine
235 in the extracellular space during degranulation.

236 Next, we probed MSPC-KA for NLRP3 and confirmed that some MC granules also contained
237 this sensor protein **(Figure 4b and inset)** and released it during degranulation. NLRP3 was
238 frequently localized at the periphery of cytoplasmic granules and at the plasma membrane in
239 degranulating MCs **(Figure 4b)**, in agreement with a recently published study showing a role
240 for NLRP3 in granule exocytosis[20]. Electron tomography on double-labeled sections revealed
241 that NLRP1^{A66V} and NLRP3 can colocalize to some, but not all MC granules **(Figure S3c-e,**
242 **Movie S1)**. This raises the possibility of compartimentalisation of inflammasome pathways
243 within MCs, but further clarification was impossible due to variations in labeling efficiencies
244 between the different primary and secondary antibodies used. Finally, triple-labeling revealed
245 that both sensor proteins can colocalize with IL1β, in both intra- and extracellular MC granules
246 **(Figure 4c-e, Movie S2)**.

247 Taken together, these findings confirm that multiple inflammasome sensor proteins can
248 simultaneously inhabit MC granules and consequently may act in tandem during activation of
249 MCs in MSPC-KAs.

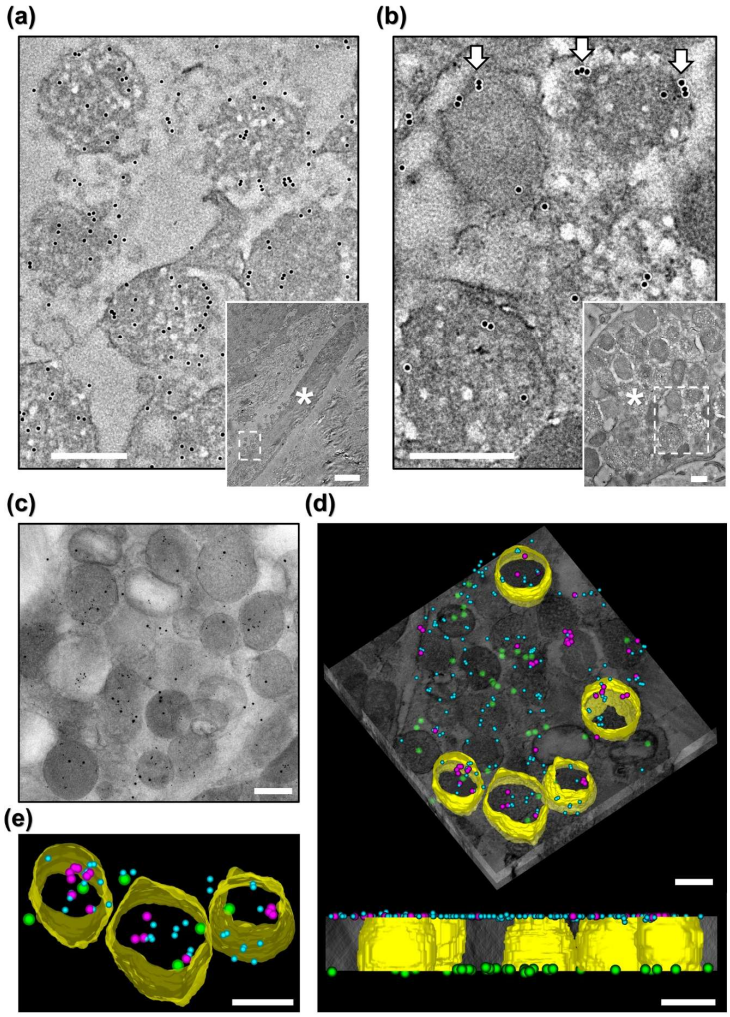

Figure 4. NLRP1^{A66V}, NLRP3 and IL1β colocalize to mast cell (MC) granules in a MSPC-keratoacanthoma. (a) High magnification of box in inset, confirming pro-IL1β/IL1β in granular material released by a MC (*). **(b)** High magnification of box in inset, showing MCs (*) contain NLRP3, which frequently localized to the periphery of granules (arrows). **(c)** Projection from tomographic tilt series, showing colocalization of gold labels (NLRP1^{A66V}, NLRP3, IL1β) in MC granules. **(d, top)** Reconstructed tomogram with superimposed contours of five MC granules (yellow), presenting colocalization of NLRP1^{A66V} (magenta), NLRP3 (turquoise) and IL1β (green). **(d, bottom)** Side-view showing distribution of labels to each side of the imaged resin section. **(e)** Detail of segmented MC granules. Scale bar for inset (a) = 2.5 µm, all others = 300 nm.

261 **DISCUSSION**

262 Here, we demonstrated that skin MCs can act as a reservoir for NLRP1, a critical but less
263 known inflammasome sensor protein. Although novel, this finding is not completely surprising,
264 as MCs express pattern recognition receptors and harbor all components of the NLRP3
265 inflammasome pathway[15], some of which are also required for NLRP1 inflammasome
266 assembly.

267 We next showed that MCs are directly involved in the pathogenesis of KAs in a MSPC patient
268 with $NLRP1^{A66V}$. In three different plantar lesions, temporally separated from initial diagnosis
269 by 1, 8 and 10 years, MCs infiltrated the epidermis and $NLRP1^{A66V}$ was released in the dermis
270 and epidermis through widespread MC degranulation.

271 KAs in MSPC develop as a consequence of pathological inflammasome activation in select
272 keratinocytes, due to mutation-induced ablation of NLRP1 auto-inhibition[7]. The fact that this
273 process is absent in hair-bearing skin despite ubiquitous skin distribution of mutant NLRP1
274 indicates highly specific triggers within the palmoplantar skin microenvironment. In our
275 samples, MC behaviour was also different between skin types. Whereas the plantar KAs
276 presented very high numbers of degranulated MCs which infiltrated the epidermis, these
277 features were conspicuously absent in a PLL lesion from the abdominal skin of the same MSPC
278 patient and also absent in KAs from 6 non-MSPC patients.

279 One possibility is that the pathological activation of MCs in MSPC-KAs is a response to
280 NLRP1-driven inflammasome activation in local keratinocytes and subsequent release of pro-
281 inflammatory factors. However, this is difficult to reconcile with two key findings: (1) that the
282 highest intensity of NLRP1 staining was in the MSPC-PLL epidermis, where keratinocytes
283 also express the hyperactive $NLRP1^{A66V}$, yet do not form KAs, and (2) that compared to healthy

284 skin, MSPC-PLL presented high numbers of MCs prone to activation by local keratinocyte
285 inflammatory cues, but these MCs had normal morphology.

286 Instead, given our finding that skin MCs harbor NLRP1, we suggest MCs as co-perpetrators of
287 MSPC-KA pathogenesis. The particular MC behaviour in the plantar skin of this MSPC patient
288 may be the result of intrinsic NLRP1-inflammasome activation in response to yet unknown
289 triggers, possibly microbial stimuli or local IgE secretion[21]. Activation of select MC clusters
290 and release of granular material would induce keratinocyte inflammatory responses, in turn
291 driving more extensive MC recruitment within the lesion (**Figure 5**).

292 In support of this, we showed that MC granular material was widely spread throughout the
293 basal and spinous layers of MSPC-KAs. These granules had higher NLRP1 content than
294 equivalents in MSPC-PLL and healthy skin and harbored NLRP3 and the pro-inflammatory
295 cytokine IL1β. The latter can be converted to its active form within intact granules via the
296 NLRP1 and NLRP3 inflammasome pathways, but also in the extracellular environment by
297 various endogenous proteases[20,22]. Regardless of the mechanism of activation, the diffusion of
298 extracellular IL1β from widespread MC degranulation could stimulate keratinocyte
299 proliferation[22]. Additionally, tryptase released during MC degranulation can cleave protease
300 activated receptor 2 (PAR-2) on the surface of keratinocytes[23], a process which stimulates non-
301 specific particle uptake through endocytosis[24]. In MSPC-KAs, this would allow enrichment of
302 keratinocytes with components of the NLRP1/NLRP3 inflammasome pathways. Even in the
303 absence of uptake of inflammasome components, other MC granule contents, like histamine,
304 serotonin and keratinocyte growth factor, are known to stimulate keratinocyte proliferation *in*
305 *situ* in mice and in human cell cultures[25,26]. The characteristic palmoplantar epidermal
306 hyperplasia in MSPC-KAs may therefore be conditioned by aberrant, NLRP1-dependent
307 activity of tissue-resident MCs.

308 This study has two important limitations. First, in absence of functional studies, we cannot
309 definitively ascertain whether MC degranulation is a prerequisite for MSPC-KA formation, or
310 if it is a local response mechanism which merely modulates lesion development. As murine
311 NLRP1 lacks the PYD domain[7], an *in vitro* experiment would be required, involving co-culture
312 of human keratinocytes with MCs expressing mutant NLRP1. Second, because we could only
313 include a single MSPC patient, carrying the $NLRP1^{A66V}$ pathogenic variant, we are unable to
314 extrapolate our findings to other MSPC variants, or generally to syndromes caused by NLRP1
315 mutations. This is further hindered by the rarity of these diseases, with only 5 MSPC families
316 known worldwide[27].
317 In summary, we showed for the first time that NLRP1 is a component of skin MC granules and
318 can colocalize with NLRP3 and IL1β, indicating that MCs have more avenues for
319 inflammasome activation than previously known. We also showed that when MCs from plantar
320 skin express $NLRP1^{A66V}$, they proliferate, infiltrate the epidermis and degranulate, contributing
321 to the pathogenesis of KAs in this variant of MSPC. This opens a new area of research in
322 NLRP1-related syndromes and, if confirmed in other patients, would translate clinically to
323 accessible therapies targeting MC activity.

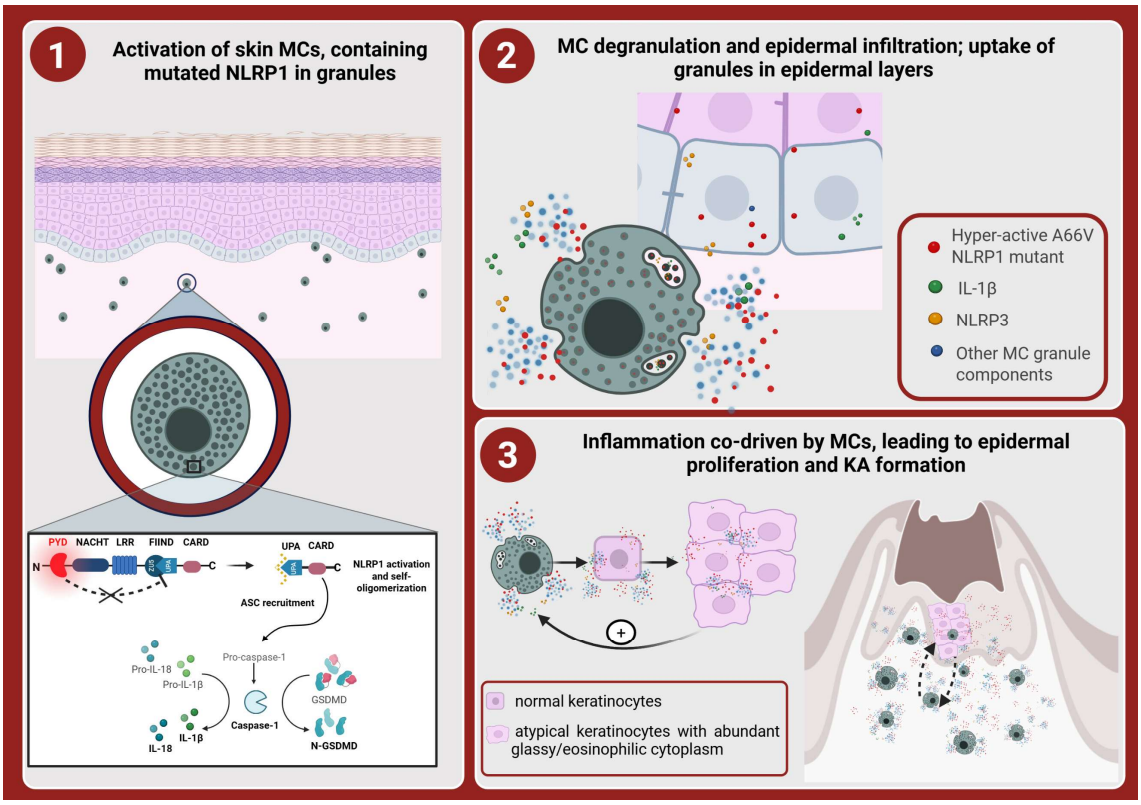

Figure 5. Potential mechanism of keratoacanthoma (KA) development in multiple self-healing palmoplantar carcinoma. Mast cells (MCs) expressing NLRP1^{A66V} proliferate and become activated in the dermis, stimulated by an unknown mechanism, possibly IL1β secretion by keratinocytes **(1)**. Constitutive activation of the NLRP1 inflammasome **(1 - inset)** leads to catastrophic degranulation of MCs. Granular material containing inflammasome components is taken up by keratinocytes up to the spinous layer **(2).** This leads to further inflammatory responses in keratinocytes and initiates a feedback loop driving activation of more MCs, which also infiltrate the lesion. Persistent inflammation induces keratinocyte hyperplasia and KA development **(3)**.

Ethics statement. The study was performed in accordance with the Declaration of Helsinki and was approved by Victor Babeș National Institute of Pathology (117/12.12.2023) and Elias University Emergency Hospital, Bucharest, Romania (122052024-2/22.05.2024). All participants provided written informed consent to participate in this study.

Data availability statement. Immunohistochemistry and transmission electron microscopy data other than presented in the article can be shared on reasonable request to the corresponding author.

Conflict of interest. The authors declare that they have no conflicts of interest.

Acknowledgments: We are grateful to the MSPC patient for participating in this study. The graphical abstract and Figure 5 were created with BioRender.com. Publication of this paper was supported by the University of Medicine and Pharmacy Carol Davila, through the institutional program Publish not Perish.

Funding: This work was supported by the Ministry of Research, Innovation and Digitalization, CCCDI - UEFISCDI, project number PN-IV-P7-7.1-PED-2024-0814, within PNCDI IV and through the National Research Authority Core Program PN-10N/2023-23.16.01.01.

Contributor statement. Conceptualization: A.D., T.E.F., R.G.P., G.C.M., D.A.I., M.G. and R.I.N.**; Data Curation:** A.D. and T.E.F.,**; Formal Analysis:** R.G.P., G.C.M., A.D., T.E.F. and A.M.C.**; Funding Acquisition:** M.G., D.A.I., G.C.M., G.T., R.I.N. and A.C.**; Investigation:** A.D., T.E.F., A.M.N., A.M.C. and R.T.A.**; Methodology:** T.E.F., A.M.N., V.E.P, D.S.M. and M.G.**; Project Administration:** T.E.F. **; Resources:** R.I.N., A.M.C. and A.M.F.**; Supervision:** A.M.F., D.A.I., M.G. and R.I.N **; Validation:** All authors**; Visualization:** A.D. and T.E.F.**; Writing – Original Draft Preparation:** A.D. and T.E.F. **; Writing – Review & Editing:** All authors**.**

357 **REFERENCES**

358 1. Martinon F, Burns K, Tschopp J. The Inflammasome: A molecular platform triggering
359 activation of inflammatory caspases and processing of proIL-β. Mol Cell [Internet]. 2002 [cited
360 2025 Jun 21];10:417–26. Available from: https://pubmed.ncbi.nlm.nih.gov/12191486/
361 2. Bauernfried S, Hornung V. Human NLRP1: From the shadows to center stage. Journal of
362 Experimental Medicine [Internet]. 2021 [cited 2025 Jun 21];219. Available from:
363 https://doi.org/10.1084/jem.20211405
364 3. Barry K, Murphy C, Mansell A. NLRP1- A CINDERELLA STORY: a perspective of recent
365 advances in NLRP1 and the questions they raise. Commun Biol [Internet]. 2023 [cited 2025
366 Jun 21];6:1–7. Available from: https://www.nature.com/articles/s42003-023-05684-3
367 4. Mitchell PS, Sandstrom A, Vance RE. The NLRP1 inflammasome: new mechanistic
368 insights and unresolved mysteries. Curr Opin Immunol [Internet]. 2019 [cited 2025 Jun
369 21];60:37–45. Available from: https://pubmed.ncbi.nlm.nih.gov/31121538/
370 5. Burian M, Schmidt MF, Yazdi AS. The NLRP1 inflammasome in skin diseases. Front
371 Immunol. 2023;14:1111611.
372 6. Calabrese L, Fiocco Z, Mellett M, Aoki R, Rubegni P, et al. Role of the NLRP1
373 inflammasome in skin cancer and inflammatory skin diseases. British Journal of Dermatology
374 [Internet]. 2024 [cited 2025 Jun 21];190:305–15. Available from:
375 https://pubmed.ncbi.nlm.nih.gov/37889986/
376 7. Zhong FL, Mamaı¨, M, Sborgi L, Saad A, Hiller S, et al. Germline NLRP1 Mutations Cause
377 Skin Inflammatory and Cancer Susceptibility Syndromes via Inflammasome Activation. Cell
378 [Internet]. 2016 [cited 2024 Apr 18];167:187–202. Available from:
379 http://dx.doi.org/10.1016/j.cell.2016.09.001
380 8. Sand J, Haertel E, Biedermann T, Contassot E, Reichmann E, et al. Expression of
381 inflammasome proteins and inflammasome activation occurs in human, but not in murine
382 keratinocytes. Cell Death Dis [Internet]. 2018 [cited 2025 Jun 21];9:1–14. Available from:
383 https://www.nature.com/articles/s41419-017-0009-4
384 9. Feldmeyer L, Keller M, Niklaus G, Hohl D, Werner S, Beer HD. The Inflammasome
385 Mediates UVB-Induced Activation and Secretion of Interleukin-1β by Keratinocytes. Current
386 Biology [Internet]. 2007 [cited 2025 Jun 21];17:1140–5. Available from:
387 https://www.sciencedirect.com/science/article/pii/S0960982207015084

388 10. Marie J, Kovacs D, Pain C, Jouary T, Cota C, et al. Inflammasome activation and
389 vitiligo/nonsegmental vitiligo progression. Br J Dermatol. 2014 Apr;170(4):816-23. doi:
390 10.1111/bjd.12691. PMID: 24734946.
391 11. Kummer JA, Broekhuizen R, Everett H, Agostini L, Kuijk L, et al. Inflammasome
392 components NALP 1 and 3 show distinct but separate expression profiles in human tissues
393 suggesting a site-specific role in the inflammatory response. Journal of Histochemistry and
394 Cytochemistry [Internet]. 2007 [cited 2025 Jun 21];55:443–52. Available from:
395 https://pubmed.ncbi.nlm.nih.gov/17164409/
396 12. Karlsson M, Zhang C, Méar L, Zhong W, Digre A, et al. A single–cell type
397 transcriptomics map of human tissues. Sci Adv [Internet]. 2021 [cited 2025 Jun 21];7.
398 Available from: https://pubmed.ncbi.nlm.nih.gov/34321199/
399 13. The Human Protein Atlas [Internet]. [cited 2025 Jun 21]. Available from:
400 www.proteinatlas.org
401 14. Nakamura Y, Kambe N, Saito M, Nishikomori R, Kim YG, et al. Mast cells mediate
402 neutrophil recruitment and vascular leakage through the NLRP3 inflammasome in histamine-
403 independent urticaria. Journal of Experimental Medicine [Internet]. 2009 [cited 2025 Jul
404 16];206:1037–46. Available from: https://pubmed.ncbi.nlm.nih.gov/19364881/
405 15. Bonnekoh H, Scheffel J, Kambe N, Krause K. The role of mast cells in
406 autoinflammation. Immunol Rev [Internet]. 2018 [cited 2025 Apr 22];282:265–75. Available
407 from: https://pubmed.ncbi.nlm.nih.gov/29431217/
408 16. Nakamura Y, Franchi L, Kambe N, Meng G, Strober W, Núñez G. Critical Role for
409 Mast Cells in Interleukin-1β-Driven Skin Inflammation Associated with an Activating
410 Mutation in the Nlrp3 Protein. Immunity [Internet]. 2012 [cited 2025 Jun 21];37:85–95.
411 Available from: https://pubmed.ncbi.nlm.nih.gov/22819042/
412 17. Kremer JR, Mastronarde DN, McIntosh JR. Computer visualization of three-
413 dimensional image data using IMOD. Journal of Structural Biology. 1996 Jan-Feb;116(1):71-
414 76. DOI: 10.1006/jsbi.1996.0013. PMID: 8742726.
415 18. Ceafalan LC, Fertig TE, Gheorghe TC, Hinescu ME, Popescu BO, et al. Age-related
416 ultrastructural changes of the basement membrane in the mouse blood-brain barrier. J Cell Mol
417 Med [Internet]. 2019 [cited 2025 Jul 16];23:819–27. Available from:
418 https://pubmed.ncbi.nlm.nih.gov/30450815/
419 19. Aguiar ALM, Martins CJ, Meuser-Batista M, Carvalho V, Barreto EO, et al. A case of
420 keratoacanthoma centrifugum marginatum with a curious mast cell accumulation at tumour

421 sites [28]. Journal of the European Academy of Dermatology and Venereology [Internet]. 2007
422 [cited 2025 Apr 26];21:429–31. Available from: https://pubmed.ncbi.nlm.nih.gov/17309493/
423 20. Mencarelli, A., Bist, P., Choi, H.W. *et al.* Anaphylactic degranulation by mast cells
424 requires the mobilization of inflammasome components. *Nat Immunol* 25, 693–702 (2024).
425 https://doi.org/10.1038/s41590-024-01788-y
426 21. Galli, S., Tsai, M. IgE and mast cells in allergic disease. *Nat Med* **18**, 693–704 (2012).
427 https://doi.org/10.1038/nm.2755
428 22. Macleod T, Berekmeri A, Bridgewood C, Stacey M, McGonagle D, Wittmann M. The
429 Immunological Impact of IL-1 Family Cytokines on the Epidermal Barrier. Front Immunol
430 [Internet]. 2021 [cited 2025 Jul 16];12:808012. Available from: www.frontiersin.org
431 23. Santulli RJ, Derian CK, Darrow AL, Tomko KA, Eckardt AJ, et al. Evidence for the
432 presence of a protease-activated receptor distinct from the thrombin receptor in human
433 keratinocytes. Proc Natl Acad Sci U S A [Internet]. 1995 [cited 2025 Jun 21];92:9151–5.
434 Available from: /doi/pdf/10.1073/pnas.92.20.9151?download=true
435 24. Benito-Martínez S, Salavessa L, Raposo G, Marks MS, Delevoye C. Melanin Transfer
436 and Fate within Keratinocytes in Human Skin Pigmentation. Integr Comp Biol [Internet]. 2021
437 [cited 2025 Jun 21];61:1546–55. Available from: https://pubmed.ncbi.nlm.nih.gov/34021340/
438 25. Maurer M, Opitz M, Henz BM, Paus R. The mast cell products histamine and serotonin
439 stimulate and TNF-α inhibits the proliferation of murine epidermal keratinocytes in situ. J
440 Dermatol Sci [Internet]. 1997 [cited 2025 Jun 21];16:79–84. Available from:
441 https://pubmed.ncbi.nlm.nih.gov/9438912/
442 26. Cho KA, Kim HJ, Kim YH, Park M, Woo SY. Dexamethasone Promotes Keratinocyte
443 Proliferation by Triggering Keratinocyte Growth Factor in Mast Cells. Int Arch Allergy
444 Immunol [Internet]. 2019 [cited 2025 Jun 21];179:53–61. Available from:
445 https://pubmed.ncbi.nlm.nih.gov/30909282/
446 27. Dobre A, Nedelcu RI, Turcu G, Brinzea A, Struna I, et al. Multiple Keratoacanthomas
447 Associated with Genetic Syndromes: Narrative Review and Proposal of a Diagnostic
448 Algorithm. Am J Clin Dermatol [Internet]. 2024 [cited 2025 Apr 19];26:45. Available from:
449 https://pmc.ncbi.nlm.nih.gov/articles/PMC11742465/

450 **SUPPLEMENTARY MATERIAL**

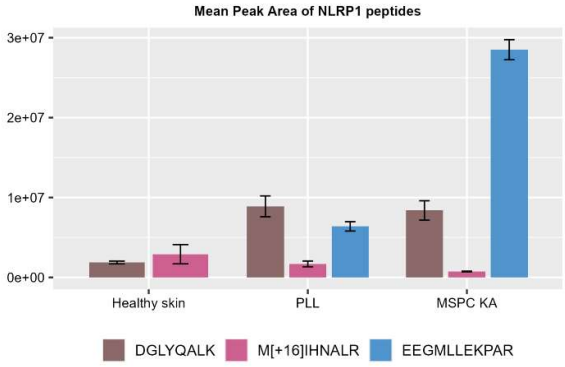

451

452 **Figure S1. Mean peak area of NLRP1 peptides identified by mass spectrometry.** Results
453 are presented as mean ± standard deviation (SD) for each peptide in healthy skin, psoriasis-like
454 lesion (PLL) and keratoacanthoma associated with multiple self-healing palmoplantar
455 carcinoma (MSPC-KA).

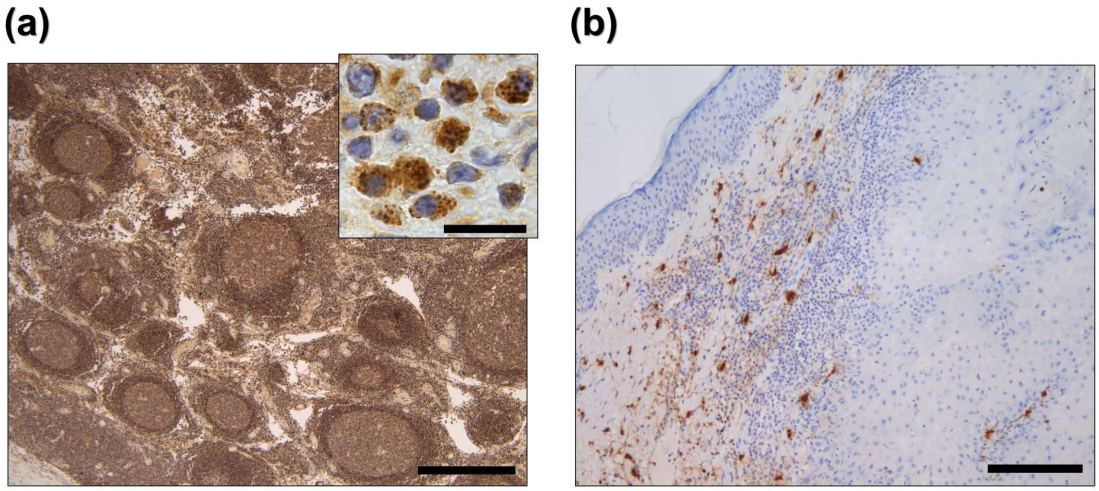

456 **Figure S2. Immunohistochemical analyses. (a)** Human lymph node stained against NLRP1,
457 showing highest proportion of positive cells in the mantle zone of lymphoid follicles. Scale bar
458 = 500 µm. Higher magnification **(inset**, scale bar = 20 µm**)** demonstrates localization of NLRP1
459 to granules of immune cells in lymph node. **(b)** Representative tryptase staining on KA from a
460 non-MSPC patient, showing absence of mast cell epidermal infiltration or degranulation. Scale
461 bar = 200 µm.

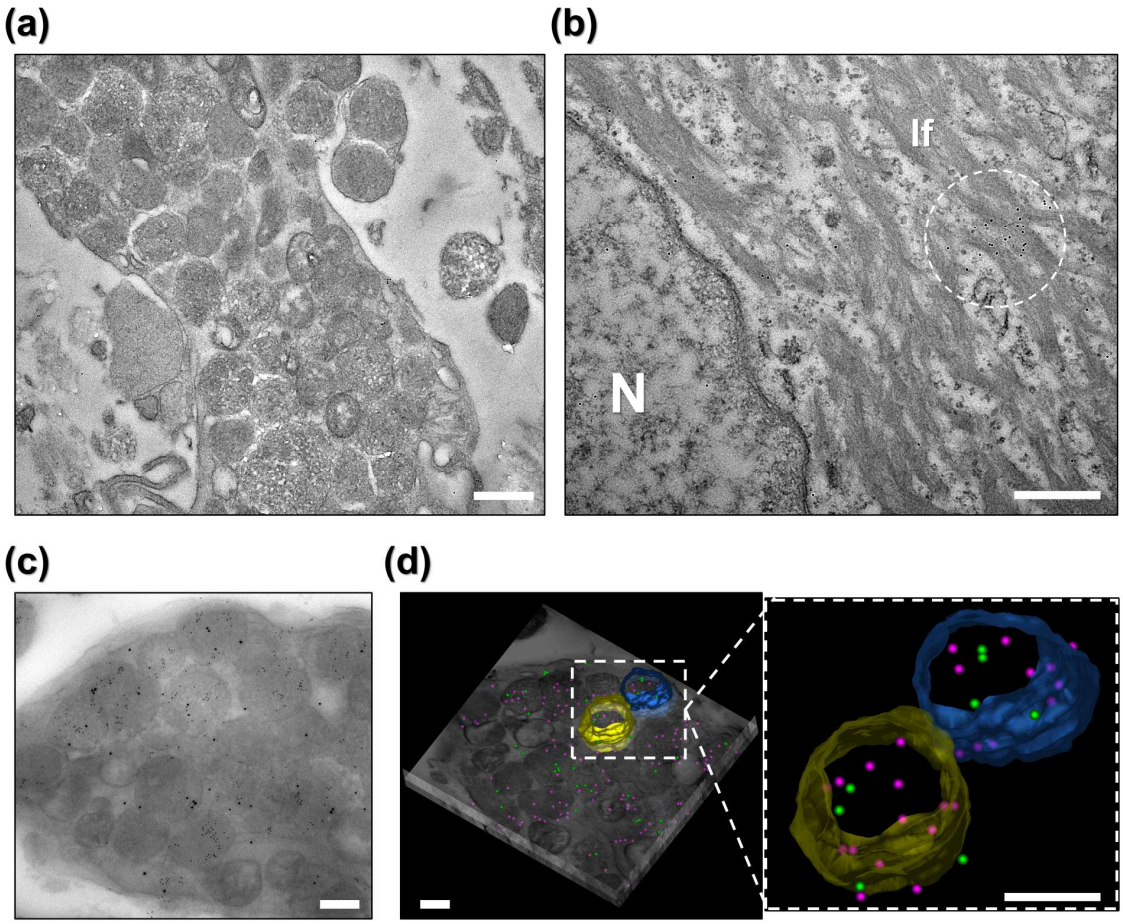

Figure S3. Immunoelectron microscopy and tomography. (a) A rabbit isotype control did not significantly bind to mast cell (MC) granules. **(b)** NLRP1 localized to intermediate filaments (If) of keratinocytes. Representative accumulation of colloidal gold can be seen as black dots (circled area). *N* - *nucleus.* **(c)** Projection from tomographic tilt series, showing colocalization of 10 and 15 nm gold particles ($NLRP1^{A66V}$ and NLRP3, respectively) in granules from a MC in MSPC-keratoacanthoma. **(d)** Reconstructed tomogram with superimposed drawn contours of two MC granules (yellow and blue), presenting colocalization of $NLRP1^{A66V}$ (magenta) and NLRP3 (green). Detail of segmented MC granules demonstrating colocalization of $NLRP1^{A66V}$ (magenta) and NLRP3 (green) are presented in the boxed area. Scale bars = 500 nm for (a-b) and 300 nm for (c-d).

473 **Table S1. Primary antibodies used for immunolabeling**

474 **Table S2. List of transitions for identified NLRP1 peptides.**

475 **Supplementary methods - mass spectrometry**

476 Biopsies were collected in cold PBS, then 50 mg from each sample was disrupted in a Mini-
477 Beadbeater (Biospec, US). Samples were then centrifuged for 20 minutes at 18,000 g and the
478 protein concentration from the supernatant was quantified by Bradford assay. A total of 50 µg
479 of protein containing supernatant was diluted with urea buffer to the final volume of 40 µL,
480 followed by the addition of 25 µL of 100 mM DTT and incubation at room temperature for 60
481 minutes. The sample was then alkylated with 26.25 µL of 300 mM iodoacetamide and kept in
482 the dark at room temperature for an additional 90 minutes followed by a quenching reaction
483 with 50 µL of DTT 100mM at room temperature for 60 minutes. The reaction mix was finally
484 diluted to 500 µL with 50 mM ammonium bicarbonate, followed by addition of trypsin (1 µg
485 /µL; Trypsin Gold, V528A, Promega, US) at a 1:50 enzyme-to-substrate ratio, with incubation
486 at 37°C for 16 hours. The reaction was stopped by adding 3 µL of formic acid. Peptides were
487 cleaned up using solid phase extraction (MonoSpin C18, GL Sciences, Japan), dried at speed-
488 vac and rehydrated to 2 µg/µL using 5% ACN + 0.1% HCOOH. Peptide concentration was
489 measured using NanoDrop 1000 (Thermo Fisher Scientific, US). From each sample, 5 µg
490 peptides were loaded into nanoACQUITY UPLC system (Waters, US) and separated using an
491 Eksigent 5C18-CL-120 (300 µM ID, 150 mm length) column coupled with a TripleTOF 5600+
492 mass spectrometer (both AB Sciex, USA). Peptide samples (5 µg) were injected using Solvent
493 A (0.1% formic acid) and separated on a 5-90% gradient Solvent B (0.1% formic acid in
494 acetonitrile) over 90 minutes, at a flow rate of 5 µL/min, with the column maintained at 55°C.
495 Each sample underwent three replicate runs. Mass spectrometric analysis was carried out using
496 electrospray ionization in positive mode, with a spray voltage of 5500 V and a source

497 temperature of 200°C. Data acquisition was performed on a TripleTOF 5600+ system in DIA
498 SWATH-MS mode, with 64 variable isolation windows. The MS1 survey scans covered an
499 m/z range of 400–1250, while MS2 spectra were collected in high-sensitivity mode from 100
500 to 2000 m/z. The accumulation period was set to 0.049 s, and ions were scanned within 55 ms
501 windows in high-sensitivity mode, giving a total cycle time of 3.5 s. Peptide and protein
502 identification were performed using PeakView 2.2, Skyline 22.2.0.255 and DIA-NN 1.9.

503 **Movie S1. NLRP1 and NLRP3 colocalize to MC granules in MSPC-KA.**

504 **Movie S2. NLRP1, NLRP3 and IL1β colocalize to MC granules in MSPC-KA.**